MDPI

Article

Tracing the Source of Hydrothermal Fluid in Ophiolite-Related Volcanogenic Massive Sulfide Deposits: A Case Study from the Italian Northern Apennines

Gabriella B. Kiss [1],*, Kata Molnár [2], Zsolt Benkó [2,3], Péter Skoda [1], Zsuzsanna Kapui [1], Giorgio Garuti [4], Federica Zaccarini [4], László Palcsu [2] and György Czuppon [5]

1   Department of Mineralogy, Institute of Geography and Earth Sciences, ELTE Eötvös Loránd University,
    1117 Budapest, Hungary
2   Isotope Climatology and Environmental Research Centre, Institute for Nuclear Research,
    4026 Debrecen, Hungary
3   Department of Mineralogy and Geology, University of Debrecen,
    4032 Debrecen, Hungary
4   Geosciences Programme, Faculty of Science, University Brunei Darussalam,
    Bandar Seri Begawan BE1410, Brunei
5   Institute for Geological and Geochemical Research, Research Centre for Astronomy and Earth Sciences,
    Eötvös Loránd Research Network, Budaőrsi út 45, 1112 Budapest, Hungary
*   Correspondence: gabriella.b.kiss@ttk.elte.hu

Abstract: The Italian Northern Apennines contain several Fe-Cu-Zn-bearing, Cyprus-type volcanogenic massive sulfide (VMS) deposits, which significantly contribute to the Cu resources of Italy. The massive sulfide lenses and related stockwork mineralizations are hosted by several levels (from basalt to serpentinite) of the unmetamorphosed ophiolitic series; therefore, this region offers perfect locations to study the ore-forming hydrothermal system in detail. A combination of fluid inclusion microthermometry, Raman spectroscopy, electron probe analyses (chlorite thermometry) and stable and noble gas isotope geochemistry was used to determine the fluid source of the VMS system at Bargone, Boccassuolo, Campegli, Casali–Monte Loreto, Corchia, Reppia and Vigonzano. This question of the fluid source is the focus of modern VMS research worldwide, as it has a direct influence on the metal content of the deposit. The obtained temperature and compositional data are both in the typical range of VMS systems and basically suggest evolved seawater origin for the mineralizing fluid. Modification of seawater was most commonly due to fluid–rock interaction processes, which happened during long-lasting circulation in the crust. The role of a small amount of magmatic fluid input was traced only at the lower block of Boccassuolo, which may be responsible for its higher ore grade. This fluid origin model is evidenced by O, H and C stable isotopic as well as He, Ne and Ar noble gas isotopic values.

Keywords: Cyprus-type VMS; Italian ophiolite; fluid inclusion study; stable isotope geochemistry; noble gas isotope geochemistry

1. Introduction

Several studies are dealing with the formation and evolution of volcanogenic massive sulfide (VMS) deposits (see, e.g., [1–5] and the references cited therein). Research projects of the past few decades provided robust genetic and descriptive models of these deposits and significantly improved our knowledge of the source of the hydrothermal fluid, the driving force of the system, the controlling factors of the ore precipitation and the transported metals. However, refinement of the models emerged new questions and challenges; a system-based approach, as well as a modern methodology, is needed to answer them.

Geological evidence generally indicates an evolved seawater origin for the hydrothermal fluid (see, e.g., 1–5 and the references cited therein), though there is a continuous

debate regarding the mode of modification, i.e., (1) fluid–rock interaction in the oceanic crust (2) and/or admixture of magmatic fluid (3) and/or phase separation may also play a role. Understanding these processes bears high importance, as they can significantly contribute to the metal content of the deposit (1% magmatic fluid component can bring 85% of the deposit's metal content [6]). However, studies on VMS deposits have shown that finding reliable evidence of the fluid source can be a challenge (see, e.g., [1,3,4] and the references cited therein). In the present study, several different mineralogical and geochemical research methods are utilized in order to better model the hydrothermal fluid source in VMS deposits through examples from the Northern Apennines, Italy. We not only show the useful combination of fluid inclusion study, Raman spectroscopy, electron probe analyses and stable and noble gas isotope analyses but also highlight those points where data interpretation may be misleading without the combination of the above-mentioned methods. Hence the obtained results can contribute to tracing the hydrothermal fluid source at other similar VMS deposits worldwide.

2. Geological Background

The Ligurian Ophiolites arrived at their present (near) surface position during the orogenesis of the Italian Apennines, beginning from the Oligocene. These ophiolites represent the remnants of the southwestern Alpine Tethys [7]. The ophiolites occurring on the eastern side of the Sestri–Voltaggio Line suffered only very low-grade metamorphism, while the ones in the Western Alps, to the west of this line, experienced high-pressure, low-temperature metamorphism. The non-metamorphosed oceanic crust fragments and the related rocks of the accretion prism form the Liguride Nappe, which is divided into two distinct units. The Internal Ligurides form the upper nappe, and its rocks are formed in a proximal position related to the spreading, whereas the External Ligurides, forming a nappe below, contain rocks representing a more distal position [7,8] (Figure 1).

The Eastern Ligurian ophiolites (where both the Internal and the External Ligurides occur) form an incomplete ophiolitic series, as the sheeted dyke complex and the transitional zone are missing or subordinate. The pillow basalt series is commonly thin (max 200 m), whereas sometimes pelagic sediments can be found on serpentinites due to syntectonic processes [8]. Based on petrological, geochemical and structural characteristics, these ophiolites formed during the early phase of oceanic crust formation, most likely related to marginal basin opening ([9,10] and the references cited therein).

Several Fe-Cu-Zn sulfide mineralizations classified as Cyprus-type volcanogenic massive sulfide deposits are known in the Eastern Ligurian ophiolites (Figure 1) [11]. These mineralizations contain 65% of the ophiolite-hosted Cu in Italy. Based on textural properties and stratigraphical position, they are divided into five groups: stratiform deposits, which occur on the top of (1) serpentinite breccia or (2) pillow basalt; stratabound deposits found (3) within the pillow basalt series; stockwork deposits, which (4) cross-cut the different units of the ophiolitic series (c: basalt, b: gabbro, a: serpentinite); and liquid magmatic massive sulfides, which (5) are hosted by serpentinite [12,13].

Modern studies of the above-mentioned deposits mostly addressed mineralogical, mineral chemical and geochemical questions (see, e.g., [11–15]), but only a little data is available about the characteristics and development of the hydrothermal process, which resulted in the ore formation [16,17]. The latter studies have shown the dynamic evolution of the fluid conditions (e.g., temperature, composition) and characterized the consecutive ore-forming and barren stages of the hydrothermal process; however, the source and development of the hydrothermal fluid remain unclear.
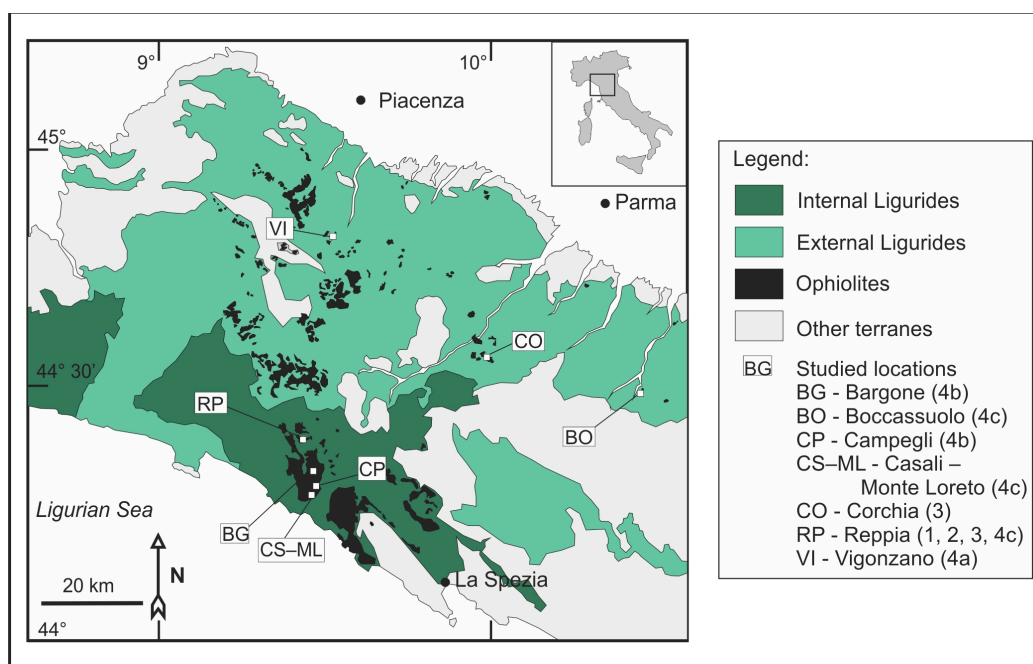
Figure 1. Simplified geological map (based on [15]) showing the ophiolites of the Northern Apennines and the study locations. Numbers refer to the deposit types introduced in Section 2.

Eight VMS locations (Figure 1) were chosen for further study from the Eastern Ligurian ophiolites, representing all hydrothermal deposit types (types 1–4abc). Vigonzano contains stockwork ore in serpentinite (4a), and Bargone and Campegli are known for their stockwork ore in gabbro (4b), while Boccassuolo, Casali, Monte Loreto and Reppia feature stockwork ore in basalt (4c); Stratabound ore in pillow basalt is known in Corchia and Reppia (3); Above this, Reppia contains stratiform sulfide in serpentinite breccia (1) and pillow basalt (2), too [12]. The most important ore minerals are chalcopyrite, pyrite, sphalerite and rarely pyrrhotite either in the massive sulfide lenses or in the stockwork ore. Local differences are observable in the gangue and accessory minerals (Table 1.).

Table 1. Mineral assemblage of the studied VMS deposits, based on the research of [13,18] and own observations.

Location	Type	Ore Minerals	Gangue Minerals	Accessories
Bargone	4b	Pyrite, chalcopyrite (sphalerite)	Quartz, prehnite (calcite, chlorite)	Bornite, covellite, Mn-minerals, Pb-selenides
Boccassuolo	4c	Pyrite, chalcopyrite, sphalerite	Quartz, calcite, chlorite, epidote, titanite	Galena, rutile, zircon
Campegli	4b	Pyrite, chalcopyrite (sphalerite)	Quartz, chlorite, epidote (pumpellyite)	Monazite, other REE minerals
Casali–Monte Loreto	4c	Pyrite, chalcopyrite sphalerite	Quartz, calcite, chlorite, epidote, titanite (actinolite, prehnite, pumpellyite)	Rutile/anatase
Corchia	3	Pyrite, chalcopyrite sphalerite, pyrrhotite	Calcite, quartz, chlorite, siderite, clay minerals, titanite	Linnéite, native gold, acanthite, uraninite, barite, REE minerals, magnetite, freibergite, galena, smithsonite, hydroromarchite
Reppia	1, 2, 3, 4c *	Pyrite, chalcopyrite, pyrrhotite (sphalerite)	Quartz, calcite, chlorite, siderite	Limonite
Vigonzano	4a	Pyrite, chalcopyrite, pyrrhotite	quartz, calcite, Chlorite, siderite, epidote, titanite, prehnite	Marcasite, millerite, chromite, magnetite, hematite, zircon, serpentine minerals

*: samples of this study represent types 1, 2 and 4c.

3. Materials and Methods

Careful fieldwork, aiming to collect representative samples, was carried out at each study location. Textural features, classification and observation of the typical features of the hydrothermal infillings were carried out with the help of a hand lens and a stereomicroscope. Further observations on the hydrothermal phenomena, as well as their host rock, were performed with a Zeiss Axioplan polarizing microscope under transmitted and

reflected light. Microphotographs were taken with the help of an Olympus Camedia C-5060 camera. These studies were performed on polished 30 μm thin sections as well as on block sections. Fluid inclusion petrography was carried out on doubly polished, 100–150 μm thick sections with an Olympus-BH2 type microscope, while the microthermometric measurements were performed by means of a Linkam FT-IR 600 type heating-freezing stage mounted on an Olympus-BX51-type microscope equipped with up to 100× long working distance objectives, providing optical magnification up to 1000×. For the calibration of the microthermometric stage, quartz-hosted synthetic CO_2 and H_2O inclusions were used, allowing 0.1 °C precision during the freezing runs and 1 °C precision during the homogenization experiments. Salinity calculations were performed based on the final ice-melting temperatures, using the equation of [19], except in inclusions with the formation of voluminous methane clathrate during the freezing runs. In these latter inclusions, the determination of salinity was based on the Raman spectra of the aqueous phase [20]. In some cases, salinity was not possible to measure due to technical reasons (metastability during freezing, small size of inclusions or strong luminescence of calcite). All the above-mentioned work was carried out at the Eötvös Loránd University, Department of Mineralogy.

Raman spectroscopy analyses of fluid inclusions were performed at the ELTE Research and Industrial Relations Center, Faculty of Science, Eötvös Loránd University, by using a Horiba Jobin Yvon LabRAM HR 800 edge filter (based confocal dispersive Raman spectrometer), with 800 mm focal length and coupled with an Olympus BXFM-type microscope. During the 3 × 20 s-long measurements, frequency-doubled Nd:YAG 532 nm laser, 600 grooves/mm grating, 50 μm confocal aperture and 50× and 100× long working distance objectives were used. The methane content of fluid inclusions was determined according to the method presented in [21]. The high-temperature Raman analyses were performed by mounting the Linkam heating-freezing stage on the microscope of the Raman equipment.

Chlorite thermometry calculations were based on electron microprobe analyses performed at the Eugen F. Stumpfl Microprobe Laboratory (University of Leoben) using a Jeol Superprobe JXA-8200, operated at 15 kV accelerating voltage, 10 nA beam current, ~1 μm beam diameter and counting times of 20 and 10 seconds for peak and backgrounds, respectively. The X-ray Kα lines for Si, Mg, Al, Ti, Cr, Ca, Na, K, Mn and Fe, as well as natural silicates and chromium spinel as standards, were used for the analysis of chlorite. Detection limits for each element are shown in the related tables. After obtaining chlorite EPMA data, we calculated its formula based on 14 O. We checked several different chlorite thermometry methods [22–27] and used the one in which criteria (Al (IV) and XFe value ranges, amount of K_2O+Na_2O+CaO, vacancy) was fulfilled by our measurement results.

Noble gas isotope analyses were carried out at the Isotope Climatology and Environmental Research Centre, Institute for Nuclear Research, Hungary. The selected rock samples were gently crushed into 0.1–5.0 mm pieces. The pure mineral (sulfide and quartz) separates were cleaned in an acetone ultrasonic bath and dried at 60 °C overnight to remove any adhering contamination. Approximately 1.0–3.5 g mineral separates were loaded into a stainless steel tube attached to the gas purification line. The gas was extracted by crushing (100 strokes) with a piston, which was activated using an external magnet. Different components of the released gas were separated in a cryogenic system consisting of two cold traps and a getter trap. Argon and the chemically active gases (e.g., O_2, CH_4, CO_2, etc.) were adsorbed in an empty trap at 25 K, while He and Ne were adsorbed in a charcoal trap at 10 K. Thereafter, Helium and Ne were desorbed at 42 and 90 K, respectively, whereas Ar was desorbed from the trap at 55 K. The isotope compositions of each noble gas were sequentially measured after purification in a getter trap (SAES) using a HELIX-SFT noble gas mass spectrometer (He) and a VG 5400 noble gas mass spectrometer (Ne, Ar). Signals were collected using a Faraday cup (^{4}He, ^{40}Ar) and an electron multiplier for the other isotopes. The overall measurement procedure was calibrated with known air aliquots and calibration gases. The measured He isotope ratios have been corrected for excess air using

the atmospheric ^{3}He/^{4}He and ^{4}He/^{20}Ne ratios, recommended by [28]. The corrections resulted in minor changes (0.01%) in the final data.

Stable carbon and oxygen isotope compositions of approximately 150–200 µg carbonate samples were determined by carrying out the carbonate–orthophosphoric acid reaction at 72 °C [29] and using an automated GASBENCH II sample preparation device attached to a Thermo Finnigan Delta Plus XP mass spectrometer at the Institute for Geological and Geochemical Research (IGGR) in Budapest, Hungary. Precision is better than ±0.1‰ for both δ^{18}O and δ^{13}C.

Stable hydrogen isotope composition of the inclusion-hosted water and the water content of carbonate (dolomite and calcite) samples were determined at the Institute for Geological and Geochemical Research (Budapest, Hungary), using the laser spectrometric method described in detail by [30,31].

4. Results

The studied mineralizations represent each level of the Cyprus-type VMS systems (massive sulfide lens and below the stockwork zone with alteration halo), although not all textural types are known at each location (see Section 2 and Table 1). A special feature of the study locations is the fact that almost every member of the ophiolitic series (basalt, gabbro and peridotite) contained mineralizations due to syntectonic processes; therefore, the studied samples cover a wide range in terms of either host rock or ore texture.

4.1. Massive Sulfide Lenses
4.1.1. Texture and Mineralogy

Massive sulfide lenses occurring in basalt and serpentinite breccia were studied in Reppia and Corchia. This type of mineralization contains more than 80% of ore minerals, including pyrite, chalcopyrite, pyrrhotite, sphalerite and detrital chromite, as well as magnetite, together with their alteration products hematite and limonite. Chlorite, quartz, calcite, clay minerals, barite and anhydrite are common gangue minerals. The gangue minerals most commonly occur among the sulfide grains, forming a massive, granular texture. However, brecciation may also occur (Figure 2).
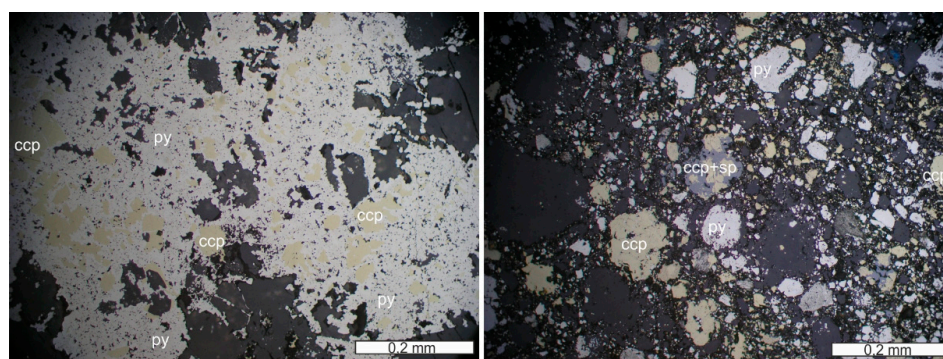

Figure 2. Massive sulfide (py—pyrite; ccp—chalcopyrite) with gangue minerals (quartz and calcite) from Corchia (reflected light microphotograph, 1N; left) and brecciated ore (pyrite, chalcopyrite; sp—sphalerite) with gangue quartz and calcite from Corchia (reflected light microphotograph, 1N; right).

The most common sulfide mineral is pyrite (50–80%), which is formed in multiple stages during the whole hydrothermal process. Pyrrhotite is formed either earlier or cogenetically with early pyrite, whereas chalcopyrite crystallizes after early pyrite. This was followed by sphalerite crystallization. Late pyrite precipitation lasted longer than chalcopyrite and sphalerite formation.

Chlorite is a common early-formed gangue mineral; the studied grains belong to the type-1 Mg–chlorite group [32] based on their composition (Table 2), and their calculated formation temperature is 198 ± 10 °C [24].

Table 2. Composition of chlorite based on EPMA data in wt.% (Det. lim.—detection limit; St. dev.—standard deviation; b.d.l.—below detection limit; n.a.—not available). Al (IV) and XFe data are based on 14 O. Formation temperature data are based on [22–24].

		Al$_2$O$_3$	MgO	K$_2$O	CaO	Cr$_2$O$_3$	Na$_2$O	MnO	SiO$_2$	TiO$_2$	NiO	FeO	Al (IV)	XFe	T (°C)
	Det. lim.	0.013	0.011	0.012	0.016	0.021	0.015	0.023	0.021	0.029	0.032	0.024			
Reppia, chlorite (*n* = 8)	Min	13.282	16.280	b.d.l.	0.077	b.d.l.	b.d.l.	0.274	29.263	b.d.l.	b.d.l.	22.194	0.824	0.392	184
	Max	17.488	18.985	0.037	0.495	b.d.l.	0.030	0.471	31.475	0.395	0.071	23.995	0.953	0.442	214
	Mean	16.172	17.606	0.035	0.263	n.a.	0.025	0.367	30.043	0.153	0.064	23.076	0.883	0.419	198
	St. dev.	1.393	1.005	0.003	0.122	n.a.	0.007	0.072	0.826	0.163	0.010	0.570	0.047	0.019	10
Campegli, chlorite (*n* = 42)	Min	15.539	13.788	0.012	0.015	b.d.l.	b.d.l.	0.279	26.578	b.d.l.	b.d.l.	11.784	0.820	0.203	222
	Max	19.979	25.644	0.062	1.258	0.206	0.059	0.819	31.758	0.199	0.141	26.950	1.147	0.515	302
	Mean	17.691	20.648	0.023	0.165	0.066	0.027	0.570	29.389	0.056	0.051	18.658	1.001	0.333	242
	St. dev.	0.858	2.873	0.015	0.211	0.052	0.014	0.165	1.234	0.042	0.025	3.766	0.082	0.074	19
Monte Loreto, chlorite (*n* = 11)	Min	14.922	14.848	0.017	b.d.l.	b.d.l.	b.d.l.	0.351	25.788	b.d.l.	b.d.l.	19.843	1.131	0.466	302
	Max	18.799	19.261	0.042	0.427	0.096	0.053	0.454	31.194	0.075	0.082	27.255	1.238	0.503	337
	Mean	18.162	15.865	0.029	0.125	0.041	0.034	0.404	26.886	0.055	n.a.	25.681	1.179	0.484	318
	St. dev.	1.162	1.260	0.010	0.202	0.029	0.012	0.036	1.555	0.016	n.a.	2.147	0.032	0.013	10

The basalt in close proximity to the massive sulfide lens shows intensive alteration. Hydrothermal veins are common, and due to the appearance of strongly altered rock-forming minerals, only the relict texture of the original rock is observable. Chlorite, albite and titanite are the most common alteration products in the host rock, whereas quartz, calcite and the above-mentioned sulfides are found in the veins.

4.1.2. Fluid Characteristics

Quartz and calcite are found among the sulfide grains. The coarser-grained quartz could be associated with later sulfides, while fine-grained quartz and calcite are clearly later products. Both may contain common ~5 μm-sized primary fluid inclusions in 3D clouds, far from any secondary plains. The observed constant phase ratio (~10 area% vapor (V) and ~90 area% liquid phase (L), though a rare, accidentally trapped mineral solid phase (S) occurs) suggests trapping from a homogeneous parent liquid (Appendix B, Figure A1). The homogenization temperature was Th(LV-L) = 127–178 °C in coarser-grained quartz (*n* = 48), Th(LV-L) = 69–91 °C in fine-grained quartz (*n* = 6) and Th(LV-L) = 49–93 °C in late calcite (*n* = 26). The salinity was rather stable with values between 2.12–4.18 NaCl equiv. wt.% (Appendix B, Figure A2). Raman spectroscopy identified methane in the vapor phase of each inclusion, and the accidentally trapped mineral was found to be sericite. Where methane content was quantified, 0.3 ± 0.05 mol/kg was calculated. Based on the above-mentioned data, a homogenization pressure of 59 ± 5 MPa was calculated [33] (Appendix A, Table A1).

4.1.3. Stable and Noble Gas Isotopic Composition

The average stable isotopic composition of the fluid inclusions occurring in quartz crystals of Corchia is $\delta D = -42.39$‰, while the average composition of calcite is $\delta^{13}C_{PDB} = -2.376$ and $\delta^{18}O_{SMOW} = 21.238$. The calculated [34] average oxygen isotope composition of fluid in equilibrium with calcite is $\delta^{18}O_{SMOW} = 0.275$ (*n* = 9) (Tables 3 and 4). To calculate this, we have used the temperature value obtained from the fluid inclusion microthermometry study of the same sample (Corchia: 70 °C). The noble gas isotopic composition of sulfide-hosted fluid inclusions from Reppia is $^{20}Ne/^{36}Ar^*$ (normalized to air) = 0.756 (st. dev. = 0.1), and $^{4}He/^{36}Ar^*$ (normalized to air) = 210.445 (st. dev. = 21.1) (Appendix A, Table A2).

4.2. Stockwork Mineralizations

4.2.1. Texture and Mineralogy

Stockwork mineralizations were studied in basalt (Boccassuolo, Reppia, Casali–Monte Loreto), gabbro (Bargone, Campegli) and peridotite (Vigonzano). In Boccassuolo, the ore veins occur in two major blocks, separated by a subvertical, NW–SE-trending fault. In Reppia, the connection between the stockwork and massive sulfide ores is difficult to observe due to tectonic processes.

Table 3. Stable isotope geochemistry of late calcite and the calculated [34] composition of the fluid in equilibrium with calcite.

Location		Calcite		Fluid
		δ^{13} C$_{PDB}$	δ^{18} O$_{SMOW}$	δ^{18} O$_{SMOW}$
Bargone (*n* = 9)	Min	−2.79	15.18	−0.32
	Max	−0.26	16.52	0.99
	Mean	−1.04	15.89	0.38
	St. dev.	0.8	0.43	0.43
Boccassuolo (upper block, *n* = 8)	Min	−0.79	15.87	−3.67
	Max	−0.01	18.51	−1.07
	Mean	−0.21	16.63	−2.92
	St. dev.	0.28	0.83	0.81
Boccassuolo (lower block, *n* = 6)	Min	0.14	22.01	3.57
	Max	0.71	22.74	4.28
	Mean	0.37	22.38	3.94
	St. dev.	0.21	0.29	0.28
Corchia (*n* = 9)	Min	−3.07	20.92	−0.04
	Max	−1.85	21.76	0.78
	Mean	−2.38	21.24	0.28
	St. dev.	0.46	0.39	0.39
Monte Loreto (*n* = 7)	Min	−6.96	14.97	0.46
	Max	−0.88	15.95	1.42
	Mean	−3.75	15.43	0.91
	St. dev.	2.96	0.42	0.41

Table 4. Results of the H isotope geochemical analyses of quartz-hosted fluid inclusions.

	δD
Bargone, quartz	−39.38 −47.01
Boccassuolo (upper block), quartz	−41.15
Boccassuolo (lower block), quartz	−65.12 −42.99 −47.14
Corchia, quartz	−42.39
Monte Loreto, quartz	−44.05
Vigonzano, quartz	−40.85 −30.39

This stockwork type of mineralization contains less than 20% sulfides; pyrite, pyrrhotite, chalcopyrite, sphalerite and galena commonly occur, but some rare minerals, such as marcasite, millerite, chromite, magnetite, bornite, covellite and Pb-selenides, may also be found. Quartz, calcite and chlorite are common gangue minerals, but clay minerals, prehnite, pumpellyite and epidote also occur (Figure 3). Details on the different steps of gangue mineral formation, as well as their relation to the ore minerals in Bargone, Boccassuolo, Campegli, Reppia and Vigonzano, are found in [16,17].

Chlorite of the stockwork veins is most commonly type 1 Mg–chlorite (nomenclature by [32]) based on their composition (Table 2). This mineral may have formed either before quartz (e.g., in Campegli gabbro, at 220–300 °C, or in Monte Loreto basalt, at 300–340 °C), syngenetically with it (e.g., in Reppia basalt, at 185–215 °C), or as a later product (e.g., at some locations of Boccassuolo, at 120–160 °C; for details on this location, see the corresponding results of [13]) [22,23].
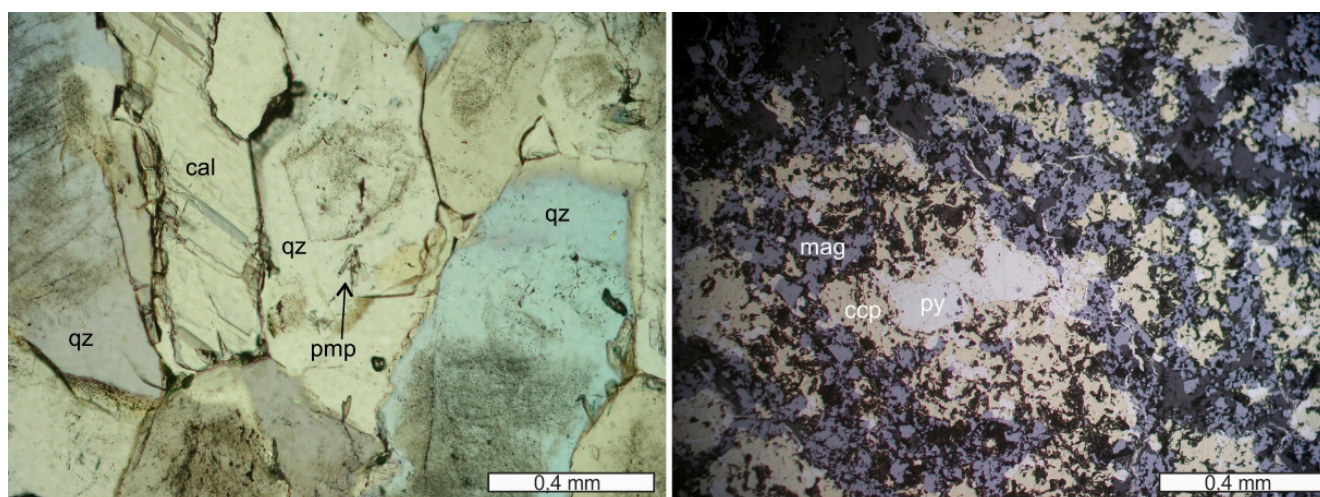
Figure 3. Coarse-grained early quartz (qz) (at places with growth zones with primary fluid inclusions), later calcite (cal) and pumpellyite (pmp) of a stockwork vein from Campegli (transmitted light microphotograph, 1N; left). Semimassive, brecciated sulfide sample of a thick quartz vein from Vigonzano, showing early pyrite (py) surrounded by later chalcopyrite (ccp), magnetite (mag) and gangue minerals (quartz). Note that pyrite can also occur in later, thin veinlets (reflected light microphotograph, 1N; right).

4.2.2. Fluid Characteristics

The fluid inclusion study was performed in different quartz generations and the late calcite, as described in [16,17]. In addition to those results, measurements were also performed in Casali–Monte Loreto. In summary of the fluid inclusion study results, the primary L+V(+S) fluid inclusions are commonly between <1 and 10 μm, occurring along growth zones of the crystals or in 3D inclusion clouds in the core of the crystals (Appendix B, Figure A1). The observed constant phase ratios suggest a homogeneous parent liquid. Based on Raman spectroscopy, sericite is the S phase, and the V phase always contains methane. The homogenization temperatures show a wide range (Th(LV-L) = 50–360 °C) (*n* = 716), depending on the study location and quartz/calcite generation. Within this range, quartz of Casali–Monte Loreto yielded a Th(LV-L) = 110–190 °C (*n* = 193) and fluid inclusions of its calcite resulted in a Th(LV-L) = 95–160 °C (*n* = 62). Slightly changeable salinity and methane content was observed at each location (2.2–9.3 NaCl equiv. wt.% salinity and 0.05–0.33 mol/kg methane), with the newly studied Casali–Monte Loreto showing results in the lower range (2.2–4.6 NaCl equiv. wt.% and 0.05–0.13 mol/kg methane) (Appendix B, Figure A2). Based on these data, the calculated homogenization pressure was between 20–50 MPa [33] (Appendix A, Table A1).

4.2.3. Stable and Noble Gas Isotopic Composition

The stable and noble gas isotopic composition of the hydrothermal minerals, as well as their fluid inclusions, were also studied. The hydrogen isotopic composition of the quartz-hosted fluid inclusions is between δD −65.12 and −30.39‰ (Table 4), while their noble gas isotopic composition is R/Ra = 0.097–0.173 (where R is the measured $^3He/^4He$ ratio, and Ra is (1.382 ± 0.006) × 10^{-6} [35]; ($^4He/^{36}Ar$)$_{air}$ = 17.126–2389.488 and ($^{20}Ne/^{36}Ar$)$_{air}$ = 0.419–5.579; Appendix A, Table A2). The stable isotopic composition of late calcite is $\delta^{18}O_{SMOW}$ = 15.0–22.7‰ and $\delta^{13}C_{PDB}$ = 0.71–(−6.96)‰ (*n* = 30). The calculated [31] oxygen isotope composition of fluid in equilibrium with calcite is $\delta^{18}O_{SMOW}$ = (−3.67)–4.28‰ (Table 3). To calculate this, we have used the temperature value obtained from the fluid inclusion microthermometry study of the same sample (Bargone: 117 °C; Boccassuolo—upper block: 80 °C; Boccassuolo—lower block: 90 °C; Monte Loreto: 128 °C).

5. Discussion

The studied Italian VMS deposits represent all levels of a Cyprus-type VMS system; therefore, we can obtain information on the formation of the massive sulfide lens as well as the stockwork ore.

5.1. Formation Conditions, Fluid Characteristics

The massive sulfide lenses form directly on the seafloor due to the rapid interaction between the hot hydrothermal fluid and the cold seawater [4]. The ore and gangue minerals commonly form together or continuously; therefore, we can obtain information on the ore genesis by studying the gangue minerals. Chlorite formed prior to the quartz, calcite and sericite and precipitated at approximately 200 °C. As homogeneous parent fluid was proven by the fluid inclusion petrography, the obtained homogenization temperature and pressure data can be interpreted as minimum formation temperatures and pressures. Thus, the following quartz and calcite precipitation occurred from a continuously cooling and low-salinity (average: 3.3 NaCl equiv. wt.%) fluid at a minimum formation temperature of 50–178 °C. This is caused by dilution and rapid cooling, depicting intensive mixing between hydrothermal fluid and seawater. The calculated minimum formation pressure (59 ± 5 MPa) is higher than the hydrostatic pressure typically affecting the massive sulfide lenses (~25 MPa [3]). This overpressure phenomenon could be caused by the rapid healing of the fluid migration pathways by newly formed hydrothermal minerals. Its result is the brecciation, well-observable in the samples.

Investigation of the relationship between the massive sulfide lenses and the stockwork mineralizations is difficult at several locations due to later tectonic processes, i.e., the obduction of the ophiolitic series. At some locations, certain levels of the system are missing, or parts of obviously different origins are close to each other (see, e.g., the different blocks of Boccassuolo). However, based on the known ore deposit model and analogies (e.g., [3,4,36] and the references cited therein), at least a distant connection between the massive sulfide lens and the stockwork zone can be assumed, and thus, we can model the processes in spite of the missing link. This connection is supported by the observed, similar hydrothermal fluid characteristics, i.e., the observable typical methane content and the similar stable and noble gas isotopic values.

Studying the gangue minerals also contributes to understanding the hydrothermal processes related to stockwork mineralization. This is well illustrated by [17], who studied quartz from Bargone, Boccassuolo, Campegli, Reppia and Vigonzano, demonstrating that combined use of fluid inclusion microthermometry, Raman spectroscopy, SEM-CL imaging and LA-ICP-MS can effectively reconstruct the physico-chemical characteristics of the hydrothermal fluid producing the barren and ore-forming stages of the evolving hydrothermal system. The additional fluid inclusion study results from Casali–Monte Loreto and the new chlorite thermometry data from Campegli, Monte Loreto and Reppia fit well into the above model; both suggest a dynamically changing hydrothermal system comprised of several consecutive steps. The calculated homogenization pressure (which can be interpreted as the minimum formation pressure due to the observed homogeneous parent fluid) is commonly found within the typical 30–60 MPa range of VMS stockwork systems [3,37]. Local variations are the results of the overpressure phenomena caused by the healing of fluid-flow pathways (fractures) by rapid precipitation of hydrothermal minerals. Therefore, pressure correction is not needed on the homogenization temperature (i.e., minimum formation temperature) data; they approximate the formation conditions well. This is also supported by the chlorite thermometry data from Reppia, where chlorite syngenetic with quartz yielded similar formation temperatures as the obtained homogenization temperatures from quartz (T_{chl} = 120–170 °C vs. T_{Qtz1-2} = 120–200 °C). An important question, however, remained open: the source of the ore-forming hydrothermal fluid.

5.2. The Source of the Hydrothermal Fluid

The obtained common temperature and compositional data (minimum formation temperature: 50–360 °C, 2.2–9.3 NaCl equiv. wt.% salinity) are both in the typical range of VMS systems and basically suggest the seawater origin of the fluid [1]. Although methane content is not common in this deposit type, it may occur [4], mostly related to abiotic processes (e.g., directly emanated from magma, thermal decay of organic material, reduction related to the serpentinization of ultramafic rocks) [38]. The interpretation of the above-shown compositional data and its variability is difficult, as several effects during its circulation could have modified the seawater. Based on the literature data, the most important influencing factors are the fluid–rock interaction during circulation in the crust, mixing with fresh seawater, phase separation (i.e., boiling), passing through evaporites in the host rock series and admixture of magmatic fluid component [1,3,39,40]. In the case of the studied deposits, phase separation and the effect of evaporitic host rock can be excluded based on the geological background as well as our fluid inclusion petrography. However, it is worth discussing the possibility and relative significance of the fluid–rock interaction processes and the magmatic fluid input. This question has both academic and economic significance and is often misinterpreted due to the difficulties of reliable proofing.

The stable O and C isotopic composition of late calcite is similar to the typical ranges of low-temperature alteration zones in VMS systems, mostly depicting fluid–rock interaction processes [4]. Results from Bargone, Boccassuolo (upper block) and Monte Loreto are in the same range (mostly between -3 and 0 $\delta^{13}C_{PDB}$; -16 and -12 $\delta^{18}O_{PDB}$), showing that the different host rock (basalt and gabbro) has a negligible effect on the stable isotopic composition. This is also supported by [41], who have found similarly enriched $\delta^{18}O$ isotopic compositions in basalt, gabbro and serpentinite of the Ligurides, indicating an exchange with lower-temperature fluids at a near-seafloor position. However, Boccassuolo (lower block) shows somewhat different characteristics (between 0–1 $\delta^{13}C_{PDB}$; -9 and -7 $\delta^{18}O_{PDB}$), pointing to slightly different fluid characteristics for that location.

In addition, the calculated oxygen isotopic composition of the fluid in equilibrium with calcite remains in the typical VMS range [1], although the effect, which has modified the original seawater, cannot be unequivocally identified (Figure 4). Similar fluid salinity and O, H stable isotopic values were interpreted to support modified seawater plus magmatic fluid admixture for VMS deposits from the Iberian Pyrite Belt [42], but we would rather beware of such an explicit conclusion. Based on our results, in the case of Boccassuolo (upper block) and Bargone, we can exclude the significant magmatic fluid input, but we cannot reliably decide whether this is the case for Monte Loreto, Corchia and Boccassuolo (lower block) results (Figure 4). The possibility of magmatic fluid involvement is the highest in the case of Boccassuolo (lower block) and the lowest at Boccassuolo (upper block). This is in good correlation with the mineralogical and geochemical observations of [15], who emphasized the effect of crustal fluid circulation and leaching in the case of the anomalously high Pb content of Boccassuolo (upper block).
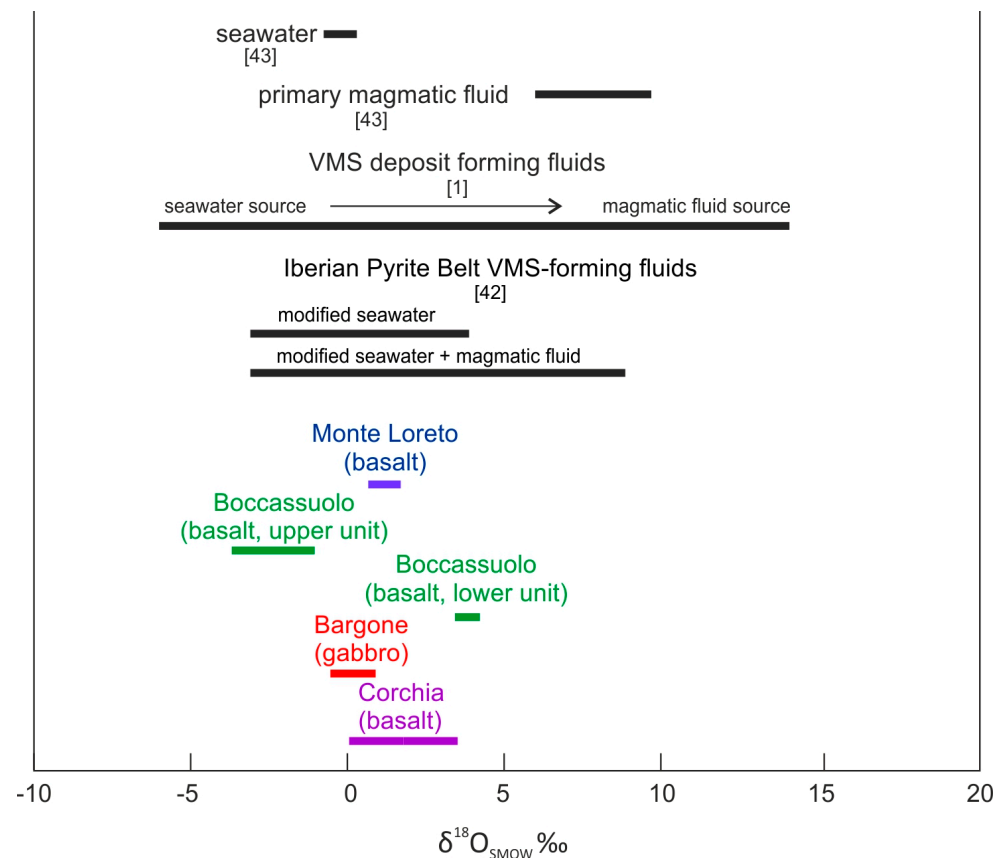
Figure 4. Stable isotopic composition of the fluid in equilibrium with late calcite from the studied locations. Reference values of [1,42,43] are shown on the top (in black) to assist interpretation.

Stable and noble gas isotopic study of quartz and sulfide-hosted fluid inclusions complete the above results. The origin of the hydrothermal fluid can be effectively traced based on the fluid inclusions of hydrothermal minerals, such as quartz and sulfides, as they are less liable to diffusion [44]. This seems to be proven in our case, too, as there is no significant difference between our results obtained from quartz and sulfides. The obtained $^{40}Ar/^{36}Ar$ data are slightly different from the atmospheric values ($^{40}Ar/^{36}Ar = 295 \pm 0.5$ [45]), showing crustal contribution [44]. Some exceptionally high values (up to 699 ± 29) can be explained by the potassium content of the commonly occurring sericite as an accidentally trapped mineral in the inclusions. The $^{4}He/^{20}Ne$, as well as the $^{4}He/^{40}Ar^*$ ratios, also support the deviation from atmospheric characteristics (Figure 5). This variance is most commonly of crustal origin, but in the case of the Boccassuolo (lower block), the magmatic (mantle) origin cannot be ruled out [44]. The ratio of He, Ne and Ar normalized to air also supports the modifying effect of fluid–rock interaction in the crust (Figure 6). However, the low R/Ra values (up to 0.17) are the unambiguous result of this process, and the mantle-derived magmatic component (which would result in higher amounts of ^{3}He) can be clearly excluded for most of the samples [44]. This is supported by the δD values (commonly between -47 and -39‰), which are within the typical VMS range [1] and show lower values than those that are characteristic of the typical field of magmatic fluids (between δD -50 and -85‰ [43]). In the case of the Boccassuolo (lower block) samples, a small amount of mantle-derived (magmatic) fluid input can be assumed based on the combined evaluation of stable isotopic (see Figure 4 and δD between -42.99 and -65.12‰) and noble gas isotopic values (Figure 5).

Summarizing our findings, we conclude that the studied Italian VMS mineralizations were formed by a seawater-originated hydrothermal fluid, in which its composition was modified by the fluid–rock interaction during its crustal circulation. The effect of the

different host rocks is negligible, which can be explained by the fact that both basalt, gabbro or serpentinite were at a near-seafloor position at the time of deposit formation due to syntectonic processes [8,41]. Only the Boccassuolo (lower block) shows different stable and noble gas isotopic compositions suggesting a slight magmatic fluid input. This finding explains the difference in the ore grade and mineralogy well; while the lower block contains medium- to high-grade ore with higher Cu and Zn values, the upper block has low- to medium-grade ore with anomalously high Pb content [15]. Thus, the appearance of high-grade ore is in correlation with the possible magmatic fluid input.
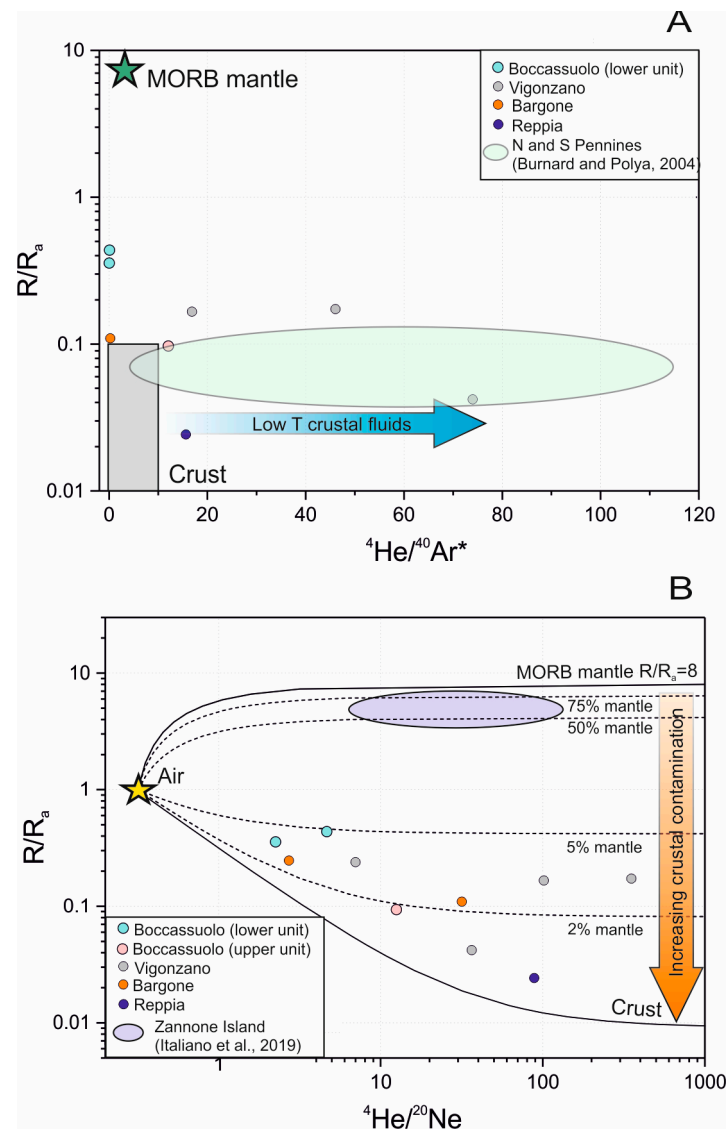

Figure 5. Interpretation of noble gas isotope composition of quartz and sulfide-hosted fluid inclusions from the studied Italian locations; $^4He/^{40}Ar^*$ (**A**) as well as $^4He/^{20}Ne$ (**B**) data both support a very slight magmatic fluid input for Boccassuolo (lower unit), while results of a fluid–rock interaction in the crust is clearly seen for the other localities (end-members in the R/Ra vs. $^4He/^{20}Ne$ plot): atmospheric (1 R/Ra, 0.318 $^4He/^{20}Ne$ [46]), crustal (0.02 R/Ra, 1000 $^4He/^{20}Ne$ [47]) and MORB (8 R/Ra, 1000 $^4He/^{20}Ne$ [48]).
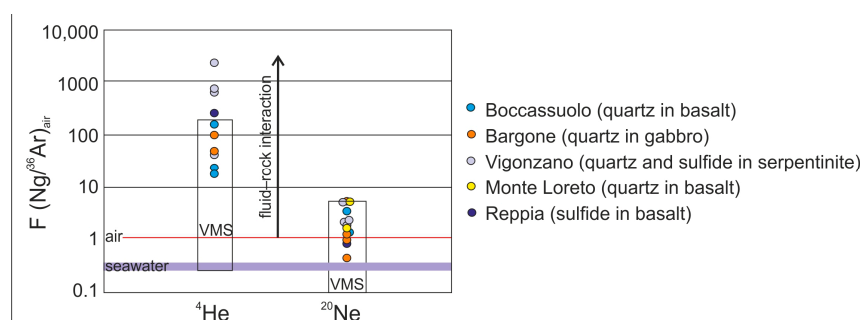
Figure 6. Noble gas isotopic composition of quartz and sulfide-hosted fluid inclusions show evidence of a fluid–rock interaction. This support the establishment of a large fluid circulation system in the crust (typical VMS fields by [44] are shown for reference).

6. Conclusions

The present research on VMS deposits of the Italian Northern Apennines has shown that the source of the VMS-forming hydrothermal fluid can be trustworthily traced by the combination of more mineralogical and geochemical study methods (namely, fluid inclusion and stable and noble gas isotopic studies). Our results support that most of the studied Italian VMS locations were formed by hydrothermal fluid of dominantly seawater origin, in which its composition evolved during long-lasting fluid–rock interaction in the crust. The only exception is the lower block of Boccassuolo, where a slight magmatic fluid input is also suggested (aside from the above-mentioned processes). This results in higher ore grades and slightly different mineralogy as well. Though the methods are well-known and often used in VMS case studies separately, a similarly complex approach is hardly available (see, e.g., [49,50]). Therefore, this novel methodology can also help other VMS locations in answering the open questions that remain.

Author Contributions: Conceptualization, G.B.K.; Methodology, G.B.K., K.M., Z.B., L.P. and G.C.; Formal analysis, G.B.K., K.M., Z.B., L.P., G.C., P.S., Z.K. and F.Z.; Investigation, G.B.K., K.M., Z.B., G.C., P.S. and Z.K.; Resources, F.Z., G.G. and G.B.K.; Writing—original draft preparation and editing, G.B.K.; Writing—review, Z.B., G.C., P.S., Z.K, F.Z. and G.G.; Visualization, G.B.K., Z.B.; Supervision, G.B.K.; Project administration, G.B.K.; Funding acquisition, G.B.K. All authors have read and agreed to the published version of the manuscript.

Data Availability Statement: All data supporting the reported results can be found in the manuscript and its appendices.

Conflicts of Interest: The authors declare no conflict of interest. The funders had no role in the design of the study; in the collection, analyses, or interpretation of data; in the writing of the manuscript; or in the decision to publish the results.

Appendix A

Table A1. Summary of primary fluid inclusion data.

		VMS Massive Sulfide				VMS Stockwork				
		Corchia	Reppia	Bargone *	Boccassuolo *	Campegli *	Casali	Monte Loreto	Reppia *	Vigonzano*
Coarse-grained quartz (Qtz 1)	T_h (°C) (core)			170–270		170–225			150–205	290–330
	T_h (°C) (rim)			135–180		125–180			120–160	260–310
	Salinity			2.6–5.7		2.6–4.7			3.1–3.9	7.2–9.3
	CH_4			x		0.13–0.22			x	x
	n			53		58			70	18
Coarse- and medium-grained quartz (Qtz 1–2)	T_h (°C)				150–360		110–180	110–190		
	salinity				3.3–8.3		3.7–4.6	2.2–3.5		
	CH_4				0.19–0.26		0.04–0.05	0.12–0.13		
	n				98		71	122		
Medium-grained quartz (Qtz 2)	T_h (°C)		127–178			110–158			122–171	
	Salinity		2.12–3.26						3.1–4.7	
	CH_4		0.32–0.34			x			0.22–0.33	
	n		48			9			41	
Fine-grained quartz (Qtz 3)	T_h (°C)	69–91		107–118	80–160				50–125	
	CH_4	?		?	x				?	
	n	6		3	15				5	
Calcite	T_h (°C)	49–93		110–135	60–160	132–169		95–156		
	Salinity	2.41–4.18		3.1–6.6						
	CH_4	x		?	x	x		?		
	n	26		13	35	6		62		

Salinity is given in NaCl equiv. wt.%. Methane content is given in mol/kg. x: methane content proven by Raman spectroscopy but not quantified. ?: methane content was not possible to check due to the small size of inclusions or strong luminescence of calcite. *: data from [16,17].

Table A2. Summary of noble gas isotope measurement data.

Locality	Sample Type	Mass (g)	3He (ccSTP/g)	St. dev. 3He	4He (ccSTP/g)	St. dev. 4He	He (ccSTP/g)	R/Ra	St. dev. R/Ra	20Ne (ccSTP/g)	St. dev. 20Ne	21Ne (ccSTP/g)	St. dev. 21Ne
Boccassuolo (stockwork basalt)	Basalt, upper block	1.58	2.29E-15	1.78E-16	1.7042E-08	1.92E-10	**1.7042E-08**	**0.0970**	0.0076	1.41E-09	3.75E-11	4.00E-12	8.37E-14
	Basalt, lower block	1.38	2.19E-15	2.05E-16	4.4485E-09	5.02E-11	**4.4485E-09**	**0.3560**	0.0336	1.98E-09	5.25E-11	5.93E-12	1.17E-13
		1.50	2.56E-15	2.07E-16	4.2420E-09	4.79E-11	**4.2420E-09**	**0.4364**	0.0356	9.11E-10	2.41E-11	2.70E-12	5.89E-14
Corchia (massive sulfide lens)		1.38	3.97E-16	2.66E-16	1.0698E-07	1.21E-09	**1.0698E-07**	**0.0268**	0.0018			3.33E-12	1.48E-13
Bargone (stockwork gabbro)		1.45	1.56E-15	1.67E-16	4.5720E-09	5.16E-11	**4.5720E-09**	**0.2465**	0.0266	1.68E-09	4.48E-11	5.35E-12	1.05E-13
		1.26	2.31E-15	2.27E-16	1.5216E-08	1.72E-10	**1.5216E-08**	**0.1095**	0.0109	4.80E-10	1.28E-11	1.41E-12	3.98E-14
		1.61	1.29E-15	1.65E-16	3.9088E-09	4.41E-11	**3.9088E-09**	**0.2390**	0.0306	5.58E-10	1.48E-11	1.63E-12	4.08E-14
Vigonzano (stockwork serpentinite)		1.38	3.33E-15	2.50E-16	5.7313E-08	6.47E-10	**5.7313E-08**	**0.0420**	0.0032	1.57E-09	4.17E-11	4.75E-12	9.69E-14
		1.48	1.37E-14	5.17E-16	5.9689E-08	6.74E-10	**5.9689E-08**	**0.1663**	0.0065	5.88E-10	1.56E-11	1.75E-12	4.44E-14
		3.41	2.11E-14	4.64E-16	8.8095E-08	9.95E-10	**8.8095E-08**	**0.1728**	0.0043	2.50E-10	6.63E-12	7.15E-13	1.80E-14
Reppia (massive sulfide lens)		2.03	7.36E-16	1.16E-16	2.1960E-08	2.48E-10	**2.1960E-08**	**0.0242**	0.0038	2.48E-10	6.57E-12	7.96E-13	2.21E-14

Locality	Sample Type	22Ne (ccSTP/g)	St. dev. 22Ne	36Ar (ccSTP/g)	St. dev. 36Ar	40Ar (ccSTP/g)	St. dev. 40Ar	Ne (ccSTP/g)	St. dev. Ne	Ar (ccSTP/g)	St. dev. Ar	20Ne/22Ne	St. dev. 20/22Ne
Boccassuolo (stockwork basalt)	Basalt, upper block	1.45E-10	4.23E-12	8.05E-10	8.49E-11			**1.56E-09**	6.98E-11			**9.766**	**0.4**
	Basalt, lower block	1.97E-10	5.73E-12	2.99E-09	2.99E-10	1.01E-06	1.07E-07	**2.18E-09**	9.60E-11	**1.02E-06**	1.48E-07	**10.041**	**0.4**
		9.23E-11	2.69E-12	1.91E-09	1.90E-10	6.13E-07	6.47E-08	**1.01E-09**	4.53E-11	**6.15E-07**	8.93E-08	**9.880**	**0.4**
Corchia (massive sulfide lens)		1.12E-10	3.28E-12										
Bargone (stockwork gabbro)		1.65E-10	4.80E-12	5.45E-10	6.04E-11			**1.85E-09**	8.16E-11			**10.215**	**0.4**
		4.69E-11	1.38E-12	1.10E-09	1.11E-10	3.85E-07	4.09E-08	**5.28E-10**	2.57E-11	**3.86E-07**	5.64E-08	**10.245**	**0.4**
		5.50E-11	1.61E-12	6.44E-10	6.64E-11	1.52E-07	1.63E-08	**6.15E-10**	2.88E-11	**1.52E-07**	2.27E-08	**10.142**	**0.4**
Vigonzano (stockwork serpentinite)		1.58E-10	4.61E-12	5.29E-10	5.37E-11	1.57E-07	1.72E-08	**1.74E-09**	7.69E-11	**1.58E-07**	2.35E-08	**9.941**	**0.4**
		6.09E-11	1.78E-12	4.58E-10	4.57E-11	1.39E-07	1.47E-08	**6.50E-10**	3.05E-11	**1.39E-07**	2.03E-08	**9.642**	**0.4**
		2.44E-11	7.13E-13	2.20E-10	2.19E-11	6.69E-08	7.05E-09	**2.75E-10**	1.29E-11	**6.71E-08**	9.74E-09	**10.235**	**0.4**
Reppia (massive sulfide lens)		2.53E-11	7.42E-13	6.26E-10	6.24E-11	1.86E-07	1.96E-08	**2.74E-10**	1.32E-11	**1.87E-07**	2.71E-08	**9.793**	**0.4**

| Locality	Sample Type	21Ne/22Ne	St. dev. 21/22Ne	40Ar/36Ar	St. dev. 40/36Ar	4He/20Ne	St. dev. 4He/20Ne	4He/40Ar *	St. dev. 4He/40Ar *	4He/36Ar * (normalized to air)	St. dev. 4He/36Ar *	20Ne/36Ar * (normalized to air)	St. dev. 20Ne/36Ar *
Boccassuolo (stockwork basalt)	Basalt, upper block	**0.028**	**0.001**			12.1	0.3			126.9	13.5	3.4	0.4
	Basalt, lower block	**0.030**	**0.001**	338.6	49.2	2.2	0.1	0.03	0.001	8.910	0.9	1.262	0.1
		0.029	**0.001**	321.1	46.6	4.7	0.1	0.09	0.003	13.337	1.3	0.913	0.1
Corchia (massive sulfide lens)		**0.030**	**0.002**										0.0
Bargone (stockwork gabbro)		**0.032**	**0.001**			2.7	0.1			50.330	5.6	5.900	0.7
		0.030	**0.001**	349.3	51.1	31.7	0.9	0.26	0.027	82.875	8.4	0.833	0.1
		0.030	**0.001**	235.9	35.1	7.0	0.2			36.422	3.8	1.657	0.2
Vigonzano (stockwork serpentinite)		**0.030**	**0.001**	297.0	44.3	36.4	1.0	73.99	3.323	650.163	66.5	5.683	0.6
		0.029	**0.001**	303.2	44.0	101.6	2.9	16.85	1.788	781.106	78.5	2.449	0.3
		0.029	**0.001**	304.2	44.2	352.6	10.2	46.05	1.604	2403.878	241.5	2.172	0.2
Reppia (massive sulfide lens)		**0.031**	**0.001**	297.7	43.2	88.6	2.6	15.64	0.540	210.445	21.1	0.756	0.1

St. dev: standard deviation.

Appendix B
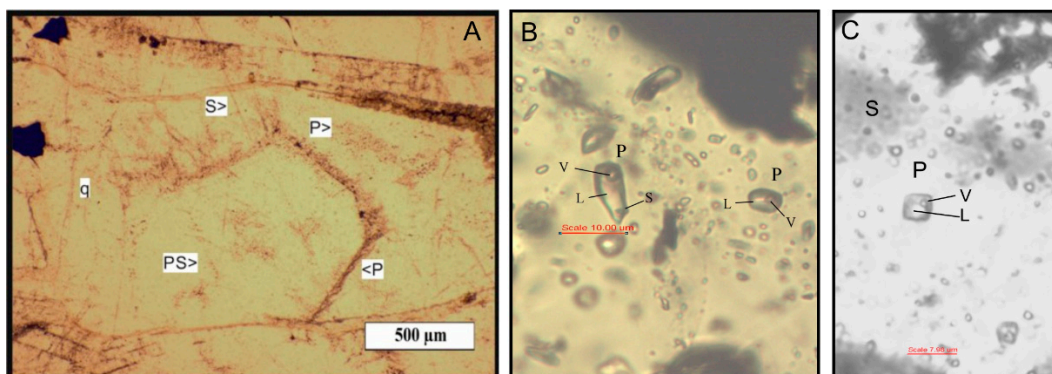
Figure A1. Microphotographs of fluid inclusions from the stratiform ore of Reppia and Corchia as well as from the stockwork ore of Casali–Monte Loreto. (**A**): location of primary (P), secondary (S) and pseudosecondary (PS) inclusions in quartz from Casali–Monte Loreto. (**B**): liquid (L), vapor (V) and accidentally trapped solid (S) containing primary inclusion in quartz from Reppia. (**C**): negative crystal-shaped two-phase inclusion in calcite from Corchia.
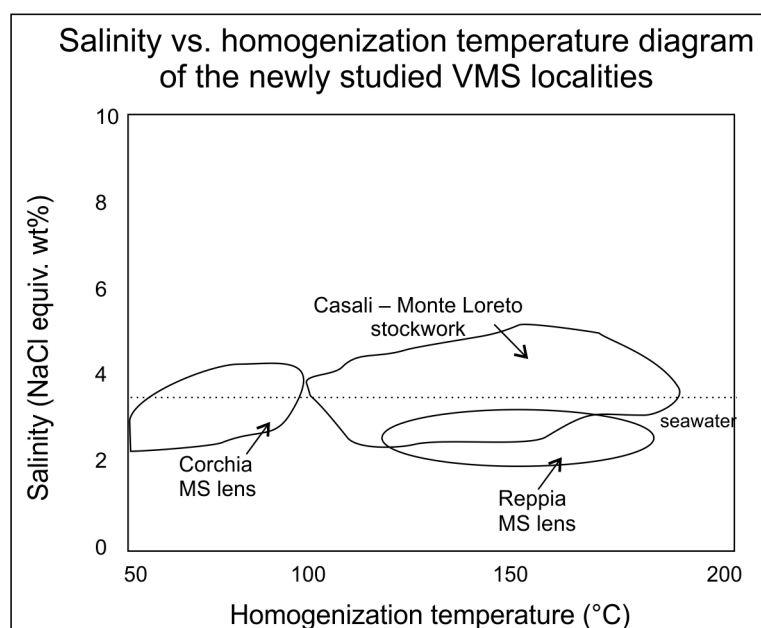

Figure A2. Salinity vs. homogenization temperature diagram of the newly studied VMS localities (quartz and calcite from the massive sulfide/MS/lenses at Corchia and Reppia and the stockwork veins of Casali–Monte Loreto).

References

1. Bodnar, R.J.; Lecumberri-Sanchez, P.; Moncada, D.; Steele-MacInnis, M. Fluid inclusions in hydrothermal ore deposits. In *Treatise on Geochemistry*, 2nd ed.; Elsevier: Oxford, UK, 2014; Volume 13, pp. 119–142.
2. Herzig, P.M.; Hannington, M.D. Polymetallic massive sulphides at the modern seafloor: A review. *Ore Geol. Rev.* **1995**, *10*, 95–115. [CrossRef]
3. Pirajno, F. *Hydrothermal Processes and Mineral Systems*; Springer: Dordrecht, The Netherlands, 2009; 1250p.
4. Shanks, W.C.P.; Thurston, R. (Eds.) *Volcanogenic Massive Sulfide Occurrence Model*; U.S. Geological Survey Scientific Investigations Report 2010–5070–C; U.S. Geological Survey: Washington, DC, USA, 2012; 345p.
5. Wilkinson, J.J. Fluid inclusions in hydrothermal ore deposits. *Lithos* **2001**, *55*, 229–272. [CrossRef]
6. Yang, K.; Scott, S.D. Magmatic sources of volatiles and metals for volcanogenic massive sulfide deposits on modern and ancient seafloors: Evidence from melt inclusions. In *Mineral Deposit Research: Meeting the Global Challenge*; Mao, J., Bierlein, F.P., Eds.; Springer: Berlin/Heidelberg, Germany, 2005; pp. 715–718.

7. Molli, G.; Crispini, L.; Mosca, P.; Piana, P.; Federico, L. Geology of the Western Alps-Northern Apennine junction area: A regional review. *J. Virtual Explor.* **2010**, *36*, 10. [CrossRef]
8. Barrett, T.J. Review of stratigraphic aspects of the ophiolitic rocks and pelagic sediments of the Vara complex, North Apennines, Italy. *Ofioliti* **1982**, *7*, 3–46.
9. Abbate, E.; Bortolotti, V.; Principi, G. Apennine ophiolites: A peculiar oceanic crust. In *Tethyan Ophiolites*; Ofioliti Special Issue; Rocci, G., Ed.; Pitagora Editrici: Bologna, Italy, 1980; Volume 1, pp. 59–96.
10. Piccardo, G.B.; Rampone, E.; Romairone, A. Formation and composition of the oceanic lithosphere of the Ligurian Tethys: Inferences from the Ligurian ophiolites. *Ofioliti* **2002**, *27*, 145–161.
11. Garuti, G.; Zaccarini, F. Assemblage and composition of Au, Ag and U minerals in Volcanic-Associated Massive Sulfide deposits of the Northern Apennine Ophiolites (Italy). *Can. Mineral.* **2005**, *43*, 935–950. [CrossRef]
12. Garuti, G.; Bartoli, O.; Scacchetti, M.; Zaccarini, F. Geological setting and structural styles of Volcanic Massive Sulphide deposits in the Northern Apennines (Italy): Evidence for seafloor and sub-seafloor hydrothermal activity in unconventional ophiolites of the Mesozoic Tethys. *Boletín Soc. Geológica Mex.* **2008**, *60*, 121–145. [CrossRef]
13. Zaccarini, F.; Garuti, G. Mineralogy and chemical composition of VMS deposits of northern Apennine ophiolites, Italy: Evidence for the influence of country rock type on ore composition. *Mineral. Petrol.* **2008**, *94*, 61–83. [CrossRef]
14. Garuti, G.; Alfonso, P.; Zaccarini, F.; Proenza, J.A. Sulfur-isotope variations in sulphide minerals from massive sulphide deposits of the Northern Apennine ophiolites: Inorganic and biogenic constraints. *Ofioliti* **2009**, *34*, 43–62.
15. Garuti, G.; Zaccarini, F.; Scacchetti, M.; Bartoli, O. The Pb-rich sulphide veins in the *Boccassuolo ophiolite*: Implications for the evolution of hydrothermal activity across the ocean-continent transition in the Ligurian Tethys (Northern-Apennine, Italy). *Lithos* **2011**, *124*, 243–254. [CrossRef]
16. Kiss, G.B. Fluid inclusion study of the Boccassuolo VMS-related stockwork deposit (Northern *Apennine ophiolites*, Italy). *Geol. Croat.* **2015**, *68*, 285–302. [CrossRef]
17. Kiss, G.B.; Bendő, Z.; Garuti, G.; Zaccarini, F.; Király, E.; Molnár, F. Reconstruction of hydrothermal processes in the Cyprus type Fe-Cu-Zn deposits of the Italian Northern Apennines: Results of combined fluid inclusion microthermometry, SEM-CL im-aging and trace element analyses by LA-ICP-MS. *Minerals* **2021**, *11*, 165. [CrossRef]
18. Bertolani, M. I giacimenti cupriferi nelle ofioliti di Sestri Levante (Liguria). *Period. Mineral.* **1952**, *21*, 149–170.
19. Hall, D.L.; Sterner, S.M.; Bodnar, R.J. Freezing point depression of NaCl-KCl-H$_2$O solutions. *Econ. Geol.* **1988**, *83*, 197–202. [CrossRef]
20. Sun, Q.; Zhao, L.; Li, N.; Liu, J. Raman spectroscopic study for the determination of Cl-concentration (molarity scale) in aqueous solutions: Application to fluid inclusions. *Chem. Geol.* **2010**, *272*, 55–61. [CrossRef]
21. Guillaume, D.; Teinturier, S.; Dubessy, J.; Pironon, J. Calibration of methane analysis by Raman spectroscopy in H$_2$O–NaCl–CH$_4$ fluid inclusions. *Chem. Geol.* **2003**, *194*, 41–49. [CrossRef]
22. Kranidiotis, P.; MacLean, W.H. Systematics of chlorite alteration at the Phelps Dodge massive sulfide deposit, Matagami, Quebec. *Econ. Geol.* **1987**, *82*, 1898–1911. [CrossRef]
23. Cathelineau, M.; Izquierdo, G. Temperature-Composition relationships of authigenic micaceous minerals in the Los Azufres geothermal system. *Contrib. Mineral. Petrol.* **1988**, *100*, 418–428. [CrossRef]
24. Zang, W.; Fyfe, W.S. Chloritization of the hydrothermally altered bedrock at the Igarapé Bahia gold deposit, Carajás, Brazil. *Miner. Depos.* **1995**, *30*, 30–38. [CrossRef]
25. Inoue, A.; Meunier, A.; Patrier-Mas, P.; Rigault, C.; Beaufort, D.; Vieillard, P. Application of chemical geothermometry to low-temperature trioctahedral chlorites. *Clays Clay Mineral.* **2009**, *57*, 371–382. [CrossRef]
26. Bourdelle, F.; Parra, T.; Chopin, C.; Beyssac, O. A new chlorite geothermometer for diagenetic to low-grade metamorphic conditions. *Contrib. Mineral. Petrol.* **2013**, *165*, 723–735. [CrossRef]
27. Lanari, P.; Wagner, T.; Vidal, O. A thermodynamic model for di-trioctahedral chlorite from experimental and natural data in the system MgO–FeO–Al2O3–SiO2–H2O: Applications to P–T sections and geothermometry. *Contrib. Mineral. Petrol.* **2014**, *167*, 968. [CrossRef]
28. Ballentine, C.J.; Burgess, R.; Marty, B. Tracing fluid origin, transport and interaction in the crust. *Rev. Mineral. Geochem.* **2002**, *47*, 539–614. [CrossRef]
29. Spötl, C.; Vennemann, T.W. Continuous–flow isotope ratio mass spectrometric analysis of carbonate minerals. *Rapid Commun. Mass Spectrom.* **2003**, *19*, 1004–1006. [CrossRef] [PubMed]
30. Czuppon, G.; Ramsay, R.R.; Özgenc, I.; Demény, A.; Gwalani, L.G.; Rogers, K.; Eves, A.; Papp, L.; Palcsu, L.; Berkesi, M.; et al. Stable (H, O, C) and noble-gas (He and Ar) isotopic compositions from calcite and fluorite in the Speewah dome, Kimberley region, western Australia: Implications for the conditions of crystallization and evidence for the influence of crustal-fluid mixing. *Mineral. Petrol.* **2014**, *108*, 759–775. [CrossRef]
31. Demény, A.; Czuppon, G.; Kern, Z.; Leél-Őssy, S.; Németh, A.; Szabó, M.; Tóth, M.; Wu, C.-C.; Shen, C.-C.; Molnár, M.; et al. Recrystallization-induced oxygen isotope changes in inclusion-hosted water of speleothems—Paleoclimatological implications. *Quatern. Int.* **2016**, *415*, 25–32. [CrossRef]
32. Zane, A.; Weiss, Z. A procedure for classifying rock-forming chlorites based on microprobe data. *Rend. Lincei Sci. Fis. Nat.* **1998**, *9*, 51–56. [CrossRef]

33.   Duan, Z.; Mao, S. A thermodynamic model for calculating methane solubility, density and gas phase composition of methane-bearing aqueous fluids from 273 to 523 K and from 1 to 2000 bar. *Geochim. Cosmochim. Acta* **2006**, *70*, 3369–3386. [CrossRef]

34.   Friedman, I.; O'Neil, J.R. Compilation of stable isotope fractionation factors of geochemical interest. In *Data of Geochemistry*; USGS Numbered Series, Professional Paper 440-KK; US Government Printing Office: Washington, DC, USA, 1977.

35.   Sano, Y.; Marty, B.; Burnard, P. Noble gases in the atmosphere. In *The Noble Gases as Geochemical Tracers*; Burnard, P., Ed.; Springer: Berlin/Heidelberg, Germany, 2013; pp. 17–31.

36.   Barrie, C.T.; Hannington, M.D. Introduction: Classification of VMS deposits based on host rock composition. *Rev. Econ. Geol.* **1999**, *8*, 2–10.

37.   Steele-Macinnis, M.; Han, L.; Lowell, R.P.; Rimstidt, J.D.; Bodnar, R.J. Quartz precipitation and fluid inclusion characteristics in sub-seafloor hydrothermal systems associated with volcanogenic massive sulphide deposits. *Centr. Eur. J. Geosci.* **2012**, *4*, 275–286.

38.   Etiope, G.; Schoell, M. Abiotic gas: Atypical but not rare. *Elements* **2014**, *10*, 291–296. [CrossRef]

39.   Foustoukos, D.I.; Seyfried, W.E. Fluid phase separation processes in submarine hydrothermal systems. *Rev. Mineral. Geochem.* **2007**, *65*, 213–239. [CrossRef]

40.   Nehlig, P. Salinity of oceanic hydrothermal fluids: A fluid inclusion study. *Earth Planet. Sci. Lett.* **1991**, *102*, 310–325. [CrossRef]

41.   Barrett, T.J.; Friedrichsen, H. Stable isotopic composition of atypical ophiolitic rocks from east Liguria, Italy. *Chem. Geol.* **1989**, *80*, 71–84. [CrossRef]

42.   Tornos, F. Environment of formation and styles of volcanogenic massive sulfides: The Iberian Pyrite Belt. *Ore Geol. Rev.* **2006**, *28*, 259–307. [CrossRef]

43.   Taylor, H.P., Jr. Oxygen isotope studies of hydrothermal mineral deposits. In *Geochemistry of Hydrothermal Ore Deposits*; Barnes, H.L., Ed.; Holt, Rinehart and Wiston: New York, NY, USA, 1967; pp. 109–142.

44.   Kendrick, M.A.; Burnard, P. Noble gases and halogens in fluid inclusions: A journey through the earth's crust. In *The Noble Gases as Geochemical Tracers—Advances in Isotope Geochemistry*; Burnard, P., Ed.; Springer: Berlin/Heidelberg, Germany, 2013; pp. 319–370.

45.   Nier, A.O. A redetermination of the relative abundances of the isotopes of carbon, nitrogen, oxygen, argon, and potassium. *Phys. Rev.* **1950**, *77*, 789–793. [CrossRef]

46.   Sano, Y.; Wakita, H. Geographical distribution of 3He/4He ratios in Japan: Implications for arc tectonics and incipient magmatism. *J. Geophys. Res. Solid Earth* **1985**, *90*, 8729–8741. [CrossRef]

47.   Sano, Y.; Marty, B. Origin of carbon in fumarolic gas from island arcs. *Chem. Geol.* **1995**, *119*, 265–274. [CrossRef]

48.   Graham, D.W. Noble Gas Isotope Geochemistry of Mid-Ocean Ridge and Ocean Island Basalts: Characterization of Mantle Source Reservoirs. *Rev. Mineral. Geochem.* **2002**, *47*, 247–317. [CrossRef]

49.   Yang, F.; Li, Q.; Yang, C.; Zhang, Z. A combined fluid inclusion and S–H–O–He–Ar isotope study of the Devonian Ashele VMS-type copper–zinc deposit in the Altay orogenic belt, northwest China. *J. Asian Earth Sci.* **2018**, *161*, 139–163. [CrossRef]

50.   Yang, C.; Zhang, B.; Yang, F.; Li, Q.; Wang, Y. Zircon U–Pb age, fluid inclusion, and H–C–O–He–Ar–S isotopic compositions as an index to the VMS-type mineralization: A case study from the Wulasigou polymetallic deposit, Altay Orogenic Belt, Northwest China. *J. Geochem. Expl.* **2021**, *222*, 106720. [CrossRef]